ChemPubSoc Europe
DOI: 10.1002/cphc.201500061
CHEMPHYSCHEM Articles

Influence of the Synthetic Conditions on the Structural and Electrochemical Properties of Carbon Nano-Onions

Olena Mykhailiv,[a] Andrzej Lapinski,[b] Agustin Molina-Ontoria,[c] Elzbieta Regulska,[a] Luis Echegoyen,*[c] Alina T. Dubis,[a] and Marta E. Plonska-Brzezinska*[a]

Thermal annealing of nanodiamonds with diameters of a few nanometers (in an inert atmosphere and at temperatures in the range: 1500–1800 °C) leads to the formation of carbon nano-onions (CNOs) with diameters between 5 and 6 nm, which correspond to nanostructures with six to eight graphitic layers. The resulting spherical CNO structures were thermally modified under different atmospheres and characterized by SEM, TEM, thermogravimetric analysis and spectroscopic (Raman and diffuse reflectance infrared Fourier transform/FTIR) spectroscopy. The electrochemical properties of the CNOs prepared under different conditions were determined and compared. The results reveal that the CNOs show different structures with predominant spherical "small" carbon nano-onions. The aim of this article is to investigate the impact of the CNO's synthesis conditions on the resulting structures and study the effect of further thermal modifications on the sizes, shapes and homogeneity of these carbon nanostructures.

1. Introduction

Carbon nanostructured materials are potentially useful in energy storage and conversion devices because of their favourable mechanical and electrical properties.[1] The electrical behaviour of these nanomaterials is related to their shape, size and surface area. A lot of attention has been paid to the capacitive properties of thin films of carbon nanotubes[2] and graphene[3] due to their porous structures and large surface areas. These materials exhibit properties of typical double-layer capacitors.[4] The energy storage (capacitive properties) arise mainly from the separation of electronic and ionic charges at the interfaces between the electrode materials and the electrolytes in solution and due to the nature and surface of the electrode–electrolyte interface.

Carbon nano-onions (CNOs) consist of a multilayered arrangement of closed fullerene shells with a distance between the layers of 0.335 nm.[5] It is important to note that the different synthetic methods lead to CNOs with different sizes, shapes, core types and physicochemical properties, primarily differing in the number of layers and the nature of the core.[6] The structure of the CNOs, the number of graphene layers and the distance between them, as well as the presence of defects, determine the physicochemical properties. Various methods for the synthesis of CNOs have been reported.[7–12] Most of these methods lead to CNOs with a large number of shells, and/or many byproducts and generally result in relatively low yields.[13] One of the most common procedures is based on the annealing of nanodiamonds (NDs) with diameters of a few nanometers in a He atmosphere and at temperatures in the range: 1500–1800 °C.[7a] This procedure leads to the formation of CNOs with very high yield. The diameter of the resulting CNOs is similar to the diameter of the NDs. The standard procedure proposed by Kuznetsov is based on the annealing of NDs with an average diameter of about 5 nm at 1650 °C under a He atmosphere.[7a] After annealing in an inert atmosphere, a second annealing is performed at 450 °C in an air atmosphere to remove amorphous carbon after formation of the CNOs. The resulting CNOs consist of a few spherical shells (6–8 layers), which is why they are commonly referred to as "small" spherical carbon nano-onions.

Recent studies of "small" onion-like structures have revealed their very interesting physicochemical properties. Thermogravimetric analyses of CNOs show their high thermal stability in air, even higher than that of C_{60}.[14] TEM, Raman and electron energy loss spectroscopy (EELS) studies suggest the presence of π electrons.[15] A decrease in the defect number after annealing at 1850 °C results in a corresponding increase in reflectivity and conductivity. CNOs obtained from the annealing of NDs at 1300–1800 °C also display very high values of specific surface areas between 380 and 600 $m^2 g^{-1}$.[16] The high conductivity is similar to those of carbon black (~4 $S cm^{-1}$) and other graphitic structures and is attractive for many applications,[17,18] mainly for electronics[19,20] and energy conversion and storage.[21]

[a] O. Mykhailiv, E. Regulska, Dr. A. T. Dubis, Dr. M. E. Plonska-Brzezinska
Institute of Chemistry, University of Bialystok
Hurtowa 1, 15-399 Bialystok (Poland)
E-mail: mplonska@uwb.edu.pl

[b] Dr. A. Lapinski
Institute of Molecular Physics
Polish Academy of Sciences
M. Smoluchowskiego 17
60-179 Poznan (Poland)

[c] Dr. A. Molina-Ontoria, Prof. Dr. L. Echegoyen
Department of Chemistry
University of Texas at El Paso
500 W. University Ave., El Paso
TX 7996 (USA)
E-mail: echegoyen@utep.edu

It has been reported that carbon nano-onion electrodes show a constant capacitance over a large scan range,[16,17] so CNO electrodes are polarizable. However, their conductivities strongly depend on the thermal treatment,[22] microtexture[23] and chemical nature,[24] as well as on their functionalization with other moieties.[22,25a] It has been shown, both experimentally and theoretically, that the structural modifications of CNO cages have a significant effect on the electrical double-layer properties and on the charging and discharging processes.[22–24] Although the electronic properties of carbon nano-onions and their potential application as supercapacitor electrode materials are increasingly being explored,[16,17,24,25] there are not many reports that systematically investigate the relationship between the synthetic parameters and their physicochemical properties. Some comprehensive studies of the annealing-induced structural transformations of onion-like structures have been conducted using X-ray diffraction[26,27] and Raman scattering.[28,29]

Since the structural properties of CNOs determine their electronic properties, the ability to control their structural transformations is important to obtain the desired functional properties. As already stated, the physical and electrical properties of CNOs are a function of their synthetic history. The aim of this article is to investigate the impact of the synthetic parameters on the size, shape and homogeneity of the resulting carbon nanostructures. To further improve the conductivity of carbon nano-onions, we modified the synthetic conditions, including the use of different atmospheres and other preparation conditions. The resulting CNOs are spherical *small* carbon nanostructures that conserve their concentric graphitic layers. We investigate their potential as supercapacitors and the relation between their structural and electrochemical properties. These properties are important for their further functionalization and applications.

2. Results and Discussion

2.1. Preparation and Textural Studies of CNOs under Different Conditions

To modify the electrochemical properties of CNO electrodes, we performed temperature- and atmosphere-controlled annealing experiments. It is known that annealing processes are commonly used to remove defects from carbon nanotubes, thus changing their electrical properties.[30,31] Moreover, the oxidation of carbon nanotubes removes amorphous carbon impurities, improves wetting by creating oxygen-terminated surfaces,[32] and creates bonding sites by breaking some C–C bonds.[33]

CNOs were prepared by the method proposed by Kuznetsov by annealing a 5 nm ND powder.[7a] Annealing of ultradispersed nanodiamonds was performed at 1650 or 1750 °C under a He atmosphere with a heating ramp of 20 °C min^{-1} (step 1, Table 1). The final temperature was maintained for one hour, and then the material was slowly cooled to room temperature over a period of one hour. Then, the CNOs were annealed at 450 or 750 °C under an atmosphere of N_2, CO_2 or air (step 2, Table 1).

Table 1. Table 1
CNO preparation conditions.

Step	Conditions	Sample
1	Annealing of NDs at 1650 °C (1 h under He)	CNOs(1650)-N_2
2	formed CNOs annealed at 450 °C in N_2 (1 h)	
1	Annealing of NDs at 1750 °C (1 h under He)	CNOs(1750)-N_2
2	formed CNOs annealed at 450 °C in N_2 (1 h)	
1	Annealing of NDs at 1650 °C (1 h under He)	CNOs(1650)-AIR
2	formed CNOs annealed at 450 °C in air (1 h)	
1	Annealing of NDs at 1750 °C (1 h under He)	CNOs(1750)-AIR
2	formed CNOs annealed at 450 °C in air (1 h)	
1	Annealing of NDs at 1750 °C (1 h under He)	CNOs(1750)-CO_2
2	formed CNOs annealed at 750 °C in CO_2 (1 h)	

Transmission electron microscopy (TEM) enabled detailed imaging of the CNO structures and the evolution of their curved graphitic layers as a function of annealing temperature and second annealing atmosphere. The TEM pictures of the samples under investigation are shown in Figure 1. The nanodiamond used as the starting material consists of particles

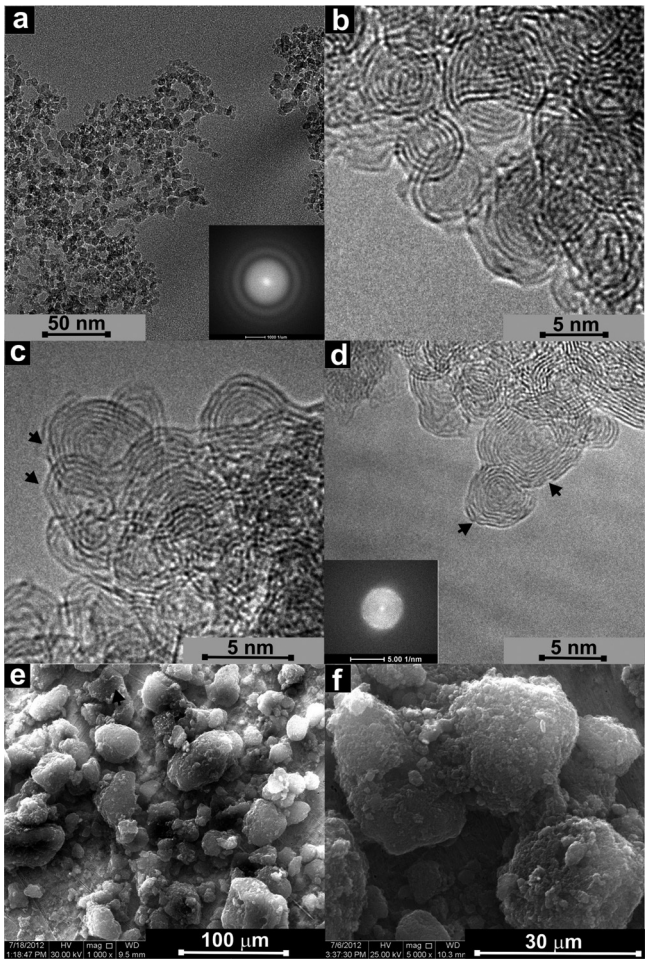

Figure 1. a–d) TEMs and e, f) SEMs of GC electrodes containing NDs (a); CNOs(1650)-AIR (b,e,f); CNOs(1750)-CO_2 (c,d).

having an average size of 5 nm (Figure 1 a). The distance between the neighboring layers is 0.206 nm, which corresponds to the (111) diamond spacing.[33] NDs were annealed at 1650 or 1750 °C for 1 h under a He atmosphere. Under these conditions, the nanodiamond samples were transformed quantitatively into CNOs (Figures 1 b–d). The number of graphitic shells ranges from a few to 12 layers. The spacing of the observed lattice for CNOs was about 0.335 nm, which was close to that of the (002) planes of graphite (Figures 1 b–d).[26] The distances of the intershell spacing estimated from TEM diffraction patterns are between 0.32 and 0.29 nm. The structural properties of the CNOs were changed as a consequence of additional annealing. This process changes the carbon structures into predominantly higher ordered graphitic layers. Some of the particles took on elliptical, polyhedral and deformed carbon nano-onion particles (Figure 1 c). This process also causes damage and structural changes on the carbon surfaces by disrupting their graphene sheet structure (Figures 1 c and 1 d). This structural modification is observed after annealing in a CO_2 atmosphere. SEM images of an Au foil covered with CNOs(1650)-AIR are shown in Figures 1 e and 1 f. All of the CNO samples prepared under different temperatures and atmospheres show a similar morphology. The CNO films exhibit porous morphologies, with many channels and outcroppings.

Differential thermogravimetric analyses (TGA-DTG-DTA) were performed to probe the thermal stability of the CNOs prepared under different atmosphere and temperature conditions. The TGA-DTG-DTA measurements were performed in an air atmosphere. Figure 2 shows the TGA-DTG-DTA curves recorded up to 1000 °C in air at 10 °C min^{-1}. The onset oxidation, inflection and the end temperatures are listed in Table 2, representing the initial weight loss, the maximum weight loss and the final weight in the TGA-DTG-DTA graphs, respectively. CNO sample degradation results from combustion of the carbon nanostructures in an air atmosphere. The thermogravimetric analyses of all of the samples were reasonably similar with the lowest thermal stability observed for the CNOs(1750)-AIR sample. Annealing under air induced structural changes by creating defects and oxygen-terminated CNO surfaces. These annealing-induced structural changes modified the spectroscopic and electrochemical properties of the CNOs.

Table 2. TGA-DTG-DTA results for CNOs annealed in different environments.

Sample	Onset temperature	Inflection temperature	End temperature
CNOs(1650)-N_2	550	670	720
CNOs(1750)-N_2	530	650	710
CNOs(1650)-AIR	500	650	700
CNOs(1750)-AIR	475	635	690
CNOs(1750)-CO_2	500	675	720

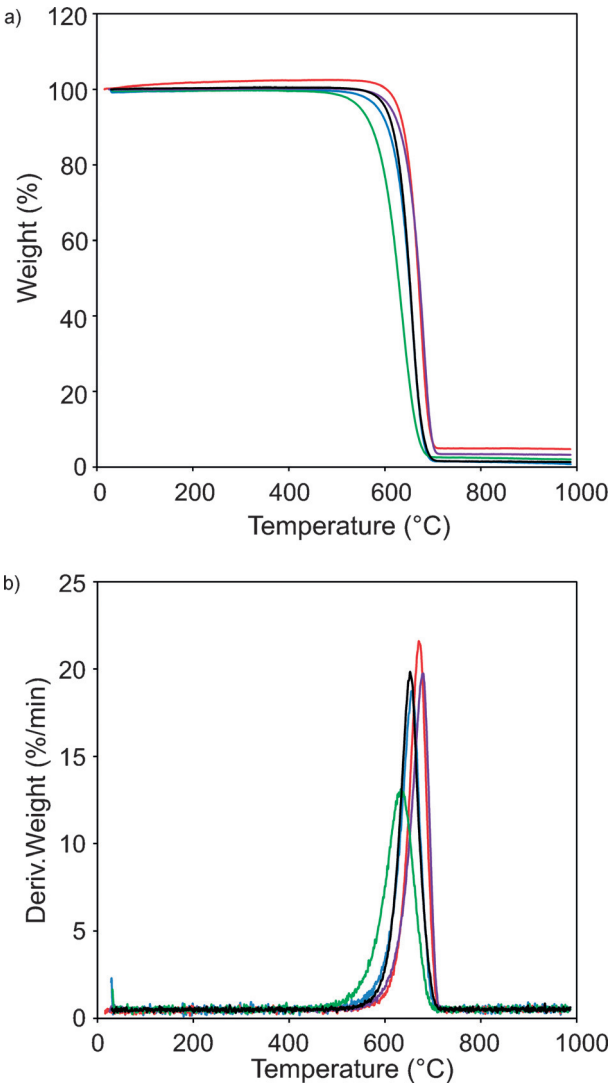

Figure 2. TGA (a) and DTG (b) curves for CNOs(1650)-N_2 (red), CNOs (1650)-CO_2 (violet), CNOs(1750)-N_2 (black), CNOs(1650)-AIR (blue), and CNOs(1750)-AIR (green). Measurement in air at 10 °C min^{-1}.

2.2. Spectral studies of CNOs

We performed Raman and FTIR studies to probe the structural characteristics of the carbon nanomaterials prepared under different atmospheres and temperatures. Figure 3 a shows the Raman spectra of one of the investigated carbon nanomaterials recorded using three different excitation lines. The first-order peaks *D*, *G*, *D′* for CNOs(1750)-AIR at 633 nm excitation are observed at 1321, 1586, and 1612 cm^{-1}, respectively. The *D* line not only changes in intensity but is also shifted as the excitation wavelengths decrease from 633 to 488 nm (see Figure 3 b).

It is known that the *D* line is dependent on the excitation wavelength for carbon nanostructures,[34–36] and is related to the double resonance Raman effect.[37–39] Other first-order peaks like the *G* and *D′* bands do not appear to have a dependence on the excitation energy (see Figure 3 b). For the other investigated compounds, the strongest features are observed at 1330–1356 (*D* line), 1582–1590 (*G* line), and 1612–1622 cm^{-1}

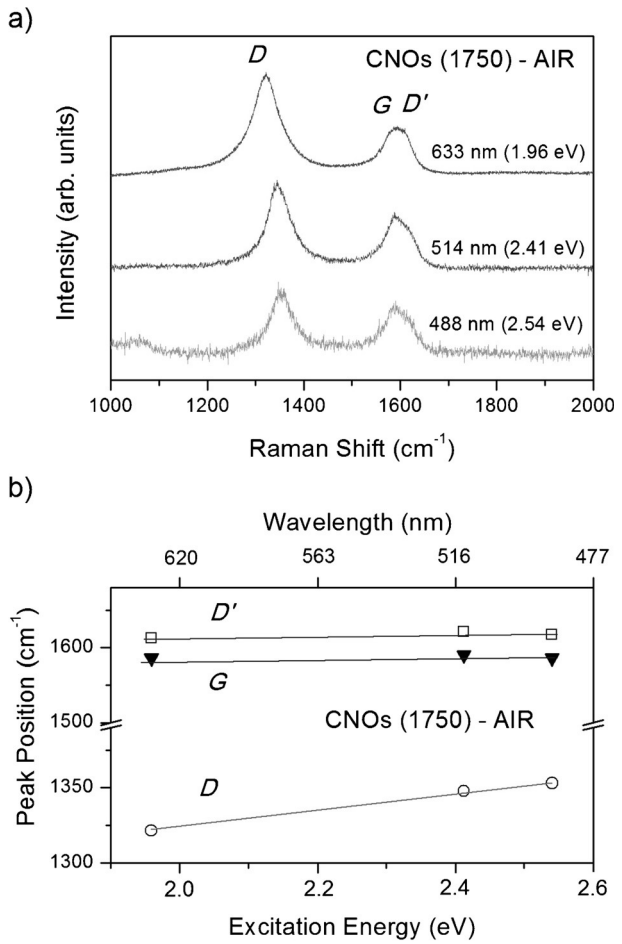

Figure 3. a) Raman spectra of CNOs(1750)-AIR recorded at 633, 514, and 488 nm. b) Effect of the excitation energy on the position of the first-order peaks for CNOs(1750)-AIR.

(D' line); and the shifts of these bands for different excitations are summarized in Table 3. For all materials, the *D* and *G* lines are intense and broad and the *D* band is stronger than the *G* band. In this respect, our spectra are similar to those of strongly disordered graphene.[40]

The *G* band is related to intramolecular vibrations between carbon atoms and the in-plane tangential stretching of the carbon–carbon bonds in graphene sheets. For single crystals of graphite, the *G* band is observed at 1580 ($\pm$5) cm^{-1} and is assigned to the E_{2g} species of the infinite crystal.[41] The position of this mode is slightly dependent on the domain size.[42] For the samples with a small crystal planar domain size L_a, a doublet structure at about 1580 cm^{-1} is observed.[42] The higher-frequency component of this doublet is observed at about 1620 cm^{-1} (D' band).[43] The D' band is a double-resonance Raman feature induced by disorder and defects, similar to the *D* band. For diamond, a single *D* band is observed at 1332 cm^{-1} and it is related to the zone-center optical phonon with F_{2g} symmetry.[44] Moreover, it is known that the Raman spectra of carbonaceous materials are very sensitive to changes that disrupt the translational symmetry. In the Raman spectrum of small graphite crystallites, the *D* band appears at about 1355 cm^{-1}.[43] This band is attributed to the A_{1g} mode of the small crystallites or to boundaries of larger crystallites of graphite. The Raman intensity of this band is inversely proportional to the crystallite size and is caused by a breakdown of the k-selection rule.[43]

The *D* and *G* bands are commonly used to characterize polymorphic carbon samples. For such materials, shifts of these modes from the typical position for planar graphite and diamond can be observed. For CNOs, it is due to the influence of bond bending on the spherical carbon shells.[45] The *D*-to-*G* intensity ratio is a convenient measure of crystalline order and in-plane crystal size. It was shown that there is a linear relationship between the *D*-to-*G* intensity ratio and the in-plane crystal size L_a obtained from X-ray data; $L_a(Å) = 44(I_D/I_G)^{-1}$.[43] The linear relationship shows that the Raman intensity is proportional to the percentage of "boundary area" in the sample. Moreover, it was shown that the *D*-to-*G* intensity ratio (I_D/I_G) is strongly dependent on the laser excitation energy.[46] Cançado et al. presented a systematic study of the dependence of the ratio between the integrated intensities of the disorder-induced *D* and *G* Raman bands (I_D/I_G) in nanographite samples with the different crystallite sizes (L_a) using different laser excitations.[48] They proposed the following general formula that allows the determination of the crystallite size L_a by Raman spectroscopy [Eq. (1)]:

$$L_a = (2.4 \times 10^{-10})\lambda_l^4 \left(\frac{I_D}{I_G}\right)^{-1} \quad (1)$$

where λ_l is the laser wavelength in nanometers.

For the investigated compounds, the ratio of the *D* and *G* band intensities (I_D/I_G) decreases from 3.18 for the 633 nm (1.96 eV) laser to 1.29 for the 488 nm (2.54 eV) (see Table 3). The changes of this ratio versus

Table 3. Best-fit frequencies ν for the *G*, *D*, and D' bands obtained for various laser excitation wavelengths, λ_{exc}, relative intensities, I_D/I_G, and corresponding average crystallite sizes, L_a.

Sample	λ_{exc} [nm]	ν_D [cm^{-1}]	ν_G [cm^{-1}]	$\nu_{D'}$ [cm^{-1}]	I_D/I_G	L_a [nm]
CNOs(1650)-N_2	633	1321	1585	1615	3.11	12.4
	514	1346	1585	1618	1.72	9.7
	488	1352	1585	1618	1.36	10.0
CNOs(1750)-N_2	633	1324	1589	1619	3.11	12.4
	514	1349	1588	1622	1.56	10.7
	488	1356	1588	1622	1.29	10.6
CNOs(1650)-AIR	633	1320	1583	1613	3.12	12.3
	514	1347	1588	1620	1.79	9.4
	488	1353	1586	1621	1.60	8.5
CNOs(1750)-AIR	633	1321	1586	1612	3.18	12.1
	514	1348	1590	1621	1.86	9.0
	488	1353	1589	1617	1.80	7.6
CNOs(1750)-CO_2	633	1322	1585	1615	2.99	12.9
	514	1347	1587	1622	1.77	9.5
	488	1353	1582	1618	1.65	8.2

the wavelength of the excitation light are related to the double-resonance Raman effect. The crystallite sizes of our samples were investigated using the formula proposed by Cançado et al.,[46] and the results are summarized in Table 3. These data show that the crystallite size, L_a, of spherical CNOs is in the range between 9–13 nm and does not depend significantly on the preparation conditions during CNO formation, although the Raman spectral profiles have been found to vary with the excitation wavelength.[46] The dependence of the Raman spectra on the excitation wavelength is interpreted in terms of π–π* resonant Raman scattering due to the presence of sp^2 carbon clusters with various sizes. Therefore, Raman scattering excited by visible radiation is more sensitive to π bonding, whereas Raman scattering excited by UV radiation is more sensitive to the σ bonding present in all carbon nanostructures.[47] In the spherical CNO nanostructures, both types of carbon atoms with sp^2 and sp^3 hybridization are present and these influence the crystallite sizes.

The CNO crystallite sizes determined by TEM (diameter ca. 5 nm) and Raman spectroscopy (diameter ca. 10 nm) are clearly very different. The larger values derived from the Raman measurements are probably the result of the phonon-confinement effect,[48] which has been observed for nanodiamond powders.[49] This effect becomes prominent when the nanocrystallites have average sizes larger than 3 nm.

Figure 4 shows the Raman spectra of CNOs(1650)-AIR and CNOs(1750)-AIR after isothermal oxidation in air at two temperatures, 1650 and 1750 °C, measured after cooling to room temperature using a 633 nm excitation wavelength. The spectra are normalized with respect to the *D* band intensity to monitor changes in the (I_D/I_G) value. This ratio is larger for higher temperatures, probably the result of more extensive oxidative damage. An increase in the line width of the *D* band (see Figure 5 and Table 4) also suggests higher disorder for the 1750 °C samples. The samples annealed at 1650 °C under a He atmosphere exhibit a *G* band that is similar to that of graphite, in contrast to those annealed at 1750 °C (see Table 3). These results indicate that CNOs(1650)-N_2 and CNOs(1650)-AIR have more graphitic structures and more ordered shells than CNOs(1750)-N_2 and CNOs(1750)-AIR. These observations are also supported by the analysis of the Raman absorption half-widths (see Table 4). A representative fit is shown in Figure 5. It can be seen that the half-width *D* and *G* bands for the 1650 °C samples are smaller than those for the 1750 °C samples, increasing the disorder in the systems. The introduction of defects is not always a disadvantage; it can be a desirable feature, especially for further functionalization due to the activation of the nanomaterial shells and the improved wetting.

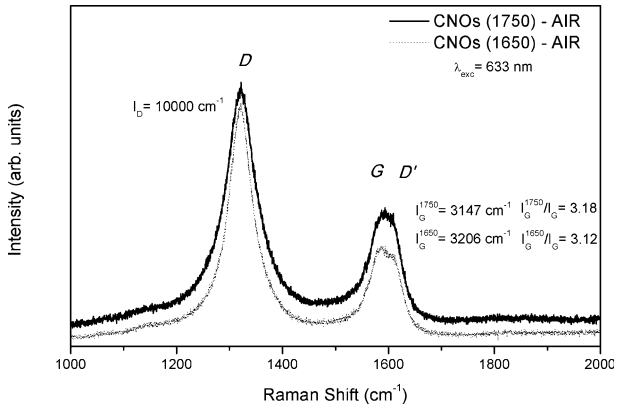

Figure 4. Raman spectra of CNOs(1750)-AIR and CNOs(1650)-AIR recorded at 633 nm. The spectra are normalized with respect to the *D* band intensity.

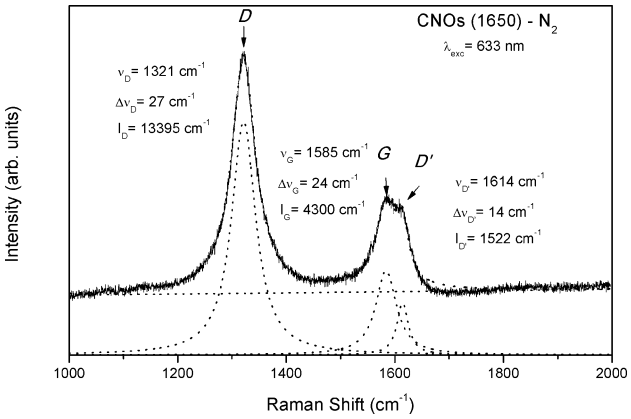

Figure 5. Raman spectra of CNOs(1650)-N_2 recorded at 633 nm and fitting of the bands with Lorentzian (Area) peaks.

Table 4. Best-fit band width $\Delta\nu$ [cm^{-1}] for the *G* and *D* bands obtained for various laser excitation wavelengths λ_{exc} [nm].

Sample	$\lambda_{exc}=633$ nm		$\lambda_{exc}=514$ nm		$\lambda_{exc}=488$ nm	
	$\Delta\nu_G$	$\Delta\nu_D$	$\Delta\nu_G$	$\Delta\nu_D$	$\Delta\nu_G$	$\Delta\nu_D$
CNOs(1650)-N_2	23.8	26.8	23.4	24.3	18.7	20.4
CNOs(1750)-N_2	27.6	36.9	26.0	29.2	25.2	28.7
CNOs(1650)-AIR	24.3	25.0	21.9	23.8	19.9	23.9
CNOs(1750)-AIR	26.6	35.0	26.3	29.4	23.1	26.9
CNOs(1750)-CO_2	25.0	26.9	22.9	22.9	20.2	23.2

Experimental[50,51] and theoretical[52] evidence clearly shows that CNOs prepared by annealing (between 800–2100 °C) of NDs possess different graphene-like structures: spherical, faceted-polyhedral or ellipsoidal. Annealing in the 1500–1800 °C temperature range leads to the creation of spherical CNO structures with six to eight graphene layers, with an interlayer distance of 0.334 nm. In the center of the nanoparticles, there is often a layer corresponding to a C_{60} molecule. The spherical product can be also converted into faceted nanoparticles upon additional annealing at higher temperatures. The resulting CNOs show various deviations from the spherical shape.

Figure 6 shows the IR spectra of CNOs prepared at 1650 or 1750 °C under nitrogen and air atmospheres. The spectra exhibit two prominent absorption bands at 1507 and 1238 cm^{-1}, which could be assigned to larger shells of the carbon nano-onions. There are also two prominent bands at 1454 and 1182 cm^{-1}, which could be identified as belonging to the innermost shell of C_{60}. The signal at 1507 cm^{-1} likely arises from an overlap of six-membered-ring contributions from fullerenes

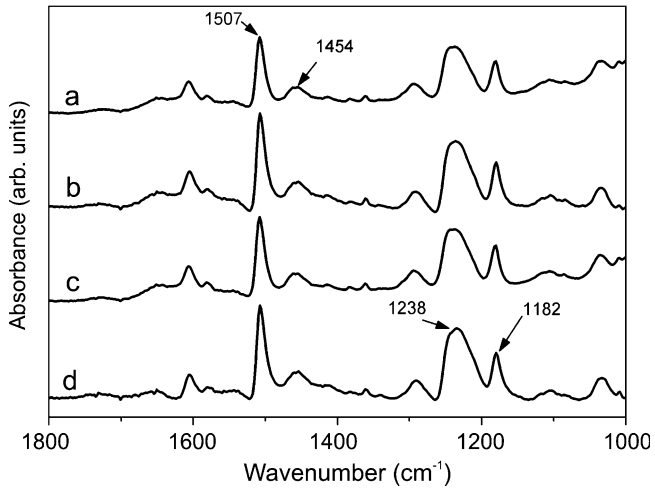

Figure 6. DRIFTS/FTIR spectra of: a) CNOs(1650)-N_2, b) CNOs(1750)-N_2, c) CNOs(1650)-AIR, and d) CNOs(1750)-AIR.

with different dimensions. The bands' half-widths at 1507 cm^{-1} indicate surface functionalization, since they were substantially broadened as a result of ozonolysis as compared to the bands of non-modified CNOs.[24] Under annealing, the intensity of the 1507 cm^{-1} band increased relative to that of the 1430 cm^{-1} band (Table 5). These changes are most likely the result of a decrease in the number of defect sites in the outer shell of the carbon nano-onions. The higher absorbance intensity ratio indicates the formation of more ordered nanostructures.

Table 5. Absorbance intensity of the larger and innermost shell bands of the samples.

Sample	I_A of the CNO band at 1507 [cm^{-1}]	I_A of the C_{60} band at 1454 [cm^{-1}]	Ratio of 1507/1454
CNOs(1650)-N_2	0.195	0.033	5.91
CNOs(1750)-N_2	0.176	0.025	7.04
CNOs(1650)-AIR	0.188	0.032	5.88
CNOs(1750)-AIR	0.175	0.026	6.73

2.3. Voltammetric Study of CNOs Obtained under Different Conditions

The electrochemical characteristics of CNOs prepared under different conditions were investigated and correlated with the nature of the CNO surfaces. To elucidate the structural effects with energy storage abilities, cyclic voltammetric studies were performed.

Due to the small size of the CNO nanoparticles (< 10 nm) and their ideal sphericity, they are referred to as zero-dimensional structures (0-D),[53] and in comparison with other carbon materials, they have better mesoporous properties, which can lead to potentially better properties for double layer capacitance (EDLCs).[54] Carbon nanostructures have been shown to be ideal materials for the easy penetration of ions at the carbon/electrolyte interface.[55] Nanoparticles with high specific surfaces are easily accessible to ions, thus exhibiting very high loading and unloading capacitive speeds.[17]

The electrochemical properties of the CNO films depend on the porous structures of the carbon surface. Annealing under a different atmosphere altered their textural properties, in agreement with the gas adsorption measurements. The micro- and mesopore structures, the pore volumes and the specific surface areas for all of the CNOs were measured and analyzed using the multilayer model of coverage adsorption, the Brunauer–Emmett–Teller (BET) static nitrogen adsorption technique.[56]

The surface area and pore volume reached maximum values of 581 $m^2 g^{-1}$ and 1.86 $cm^3 g^{-1}$, respectively, for CNOs(1750)-AIR (Table 6). Barret–Joyner–Halenda (BJH) proposed a calculation method for the distribution of pore volumes or surface areas as a function of the pore diameter using nitrogen adsorption–desorption data.[57] Based on these analyses, it is possible to determine the necessary gas volume to fill all the pores in the materials, considering their cylindrical form. Average pore sizes were also estimated from the pore volume, which is derived from the amount of N_2 vapor adsorbed at a relative pressure close to unity (t-Plot method and BJH model). The average pore size was observed to be between ~11 and ~13 nm after annealing. According to the pore-size-distribution curves of the BJH adsorption, it was also possible to estimate the pore-size distribution of the carbon nano-onions. CNOs have mainly mesoporous structures, with pores in the 2–50 nm diameter range. As shown in Table 6, there is a small fraction of micropores (< 2 nm) available in all of the CNO materials. Annealing of CNOs at 1750 °C and further additional annealing in an air atmosphere led to more micropores, and the total micropore area of the micropores significantly increased up to 418.5 $m^2 g^{-1}$ for CNOs(1750)-AIR (t-Plot method).

Table 6. Textural parameters of CNOs according to the N_2 adsorption/desorption isotherms.

Sample	S_{BET}[a] [$m^2 g^{-1}$]	Micropore area [$m^2 g^{-1}$][b]	Pore volume V_p [$cm^3 g^{-1}$][c]	Pore size [nm]
CNOs(1650)-N_2	385	37.9	1.04	10.78
CNOs(1750)-N_2	442	107.2	1.56	11.10
CNOs(1650)-AIR	488	116.3	1.56	12.79
CNOs(1750)-AIR	581	418.5	1.86	12.79
CNOs(1750)-CO_2	399	20.3	1.19	11.96

[a] S_{BET}: BET specific surface area. [b] Based on the t-Plot method. [c] Single-point adsorption, total pore volume of the pores.

For the electrochemical studies, films containing CNOs were prepared following the procedure described below. A drop of the dispersion containing CNOs was deposited on the glassy carbon (GC) electrode surface. For the preparation of the CNO films, a conductive carbon paste was used to solubilize the CNOs for further modification of the GC surface electrodes.

The volume ratio of carbon paste to ethanol was 1:6. A drop (10 mL) of the ethanol dispersion was deposited on the electrode surface. After solvent evaporation, the electrode covered with the thin film was transferred to a solution with the supporting electrolyte. The films exhibit excellent electrochemical stability under cyclic voltammetric conditions. The voltammetric responses of the CNO films obtained from different samples are shown in Figure 7. The film exhibits a stable and conductive behavior under cyclic voltammetric conditions. All the voltammograms exhibit pseudorectangular cathodic and anodic profiles that are typical for double-layer capacitors (Figures 7 and 8 b).[58] No changes of the current were observed after prolonged potential cycling between −100 and +500 mV (vs. Ag/AgCl). Therefore, the high degree of reversibility for double layers near the CNO film surface indicates that there are no chemical processes or other changes occurring between charge and discharge cycles.

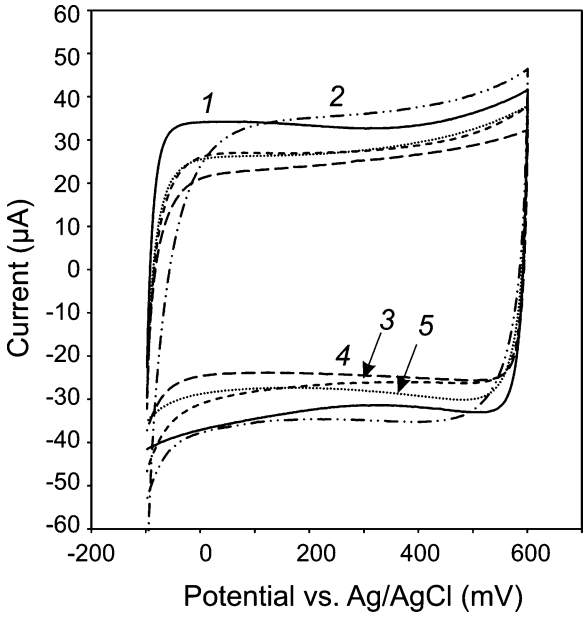

Figure 7. Cyclic voltammograms of GC electrodes containing: 1) CNOs(1650)-AIR, 2) CNOs(1750)-AIR, 3) CNOs(1650)-N_2, 4) CNOs(1750)-N_2, and 5) CNOs(1650)-N_2 in 0.1 mol L^{-1} NaCl. The sweep rate was 5 mV s^{-1}.

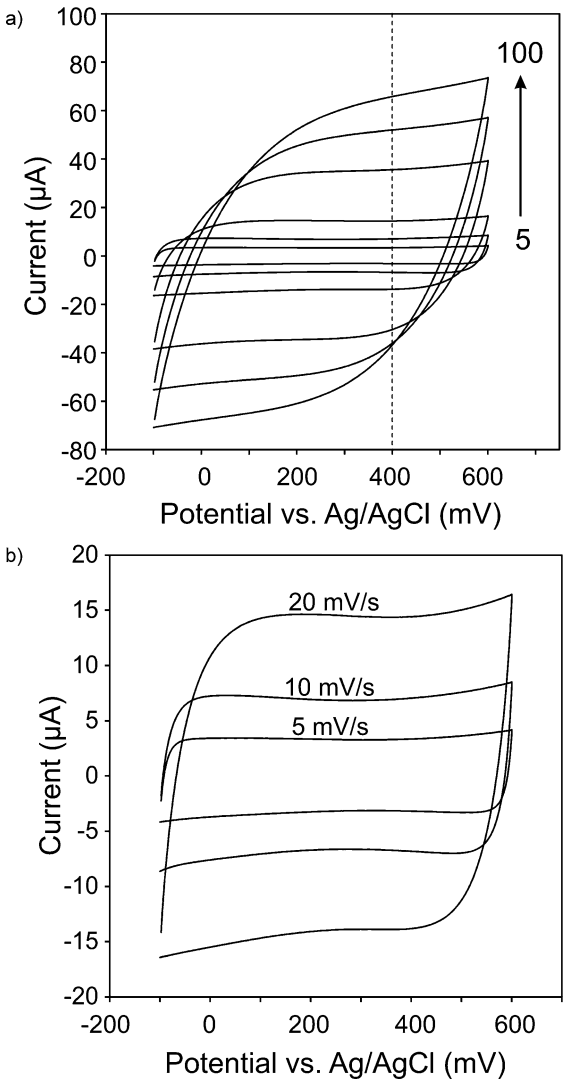

Figure 8. Cyclic voltammograms of GC electrodes of CNOs(1650)-AIR in 0.1 mol L^{-1} NaCl. The sweep rates were: 5, 10, 20, 50, 75, and 100 mV s^{-1}.

The effect of the sweep rate on the voltammograms of the CNO films was also studied (Figure 8). The rectangular CV shapes observed for all the samples over a wide range of voltage scan rates indicate a fast charge transport within the electrodes, and electrical double layer capacitance. The CV shape remained almost undistorted upon increasing the scan rate from 5 to 20 mV s^{-1}, indicating excellent wetting and easy transport of ions within the films (Figure 8). Figure 9 shows the voltammetric behavior of the CNO films in a 0.1 M NaCl aqueous solution at different potential sweep rates. The capacitive current depends linearly on the sweep rate at 400 mV (vs. Ag/AgCl) (Figure 9). The dependence of the capacitive current, i_c, over the complete range of potential scan rates is linear. These results indicate that the charge–discharge processes of the electrical double layer are highly reversible and kinetically facile. The difference between the observed capacitive current behavior for the different CNO samples is likely the result of more porous structures and more defects on the surfaces of the samples prepared under air and CO_2 atmospheres (Figure 9).

The CV traces were used to determine the specific capacitance, C_s, of the electrodes. The specific capacitance can be estimated using Equation (2), where C_s is the specific capacitance; E_1, E_2 are the cut off potentials in cyclic voltammetry; *i(E)* is the instantaneous current; *i(E)dE* is the total voltammetric charge obtained by the integration of the positive and negative sweeps in the cyclic voltammograms, *v* is the scan rate and *m* is the mass of the individual sample.[58]

$$C_S = \frac{\int_{E1}^{E2} i(E)dE}{2vm(E_2 - E_1)} \quad (2)$$

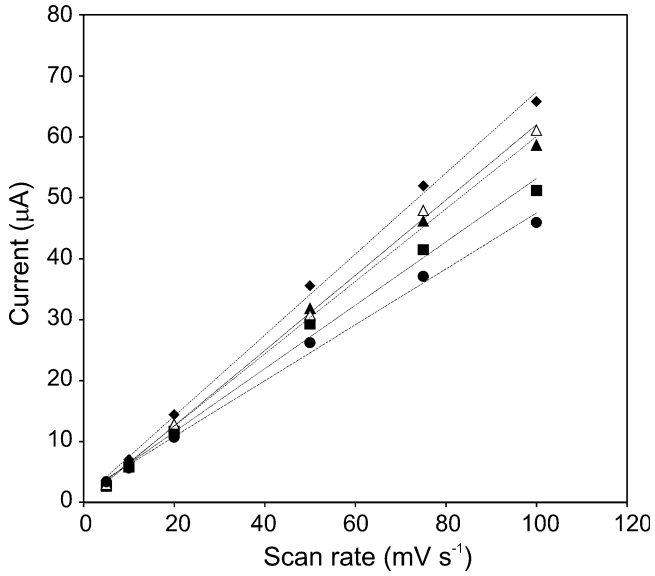

Figure 9. Dependence of the capacitive current on the sweep rate for: ■) CNOs(1650)-N_2, ▲) CNOs(1750)-N_2, Δ) CNOs 1650 °C annealed at 750 °C CO_2, ◆) CNOs(1650)-AIR, and ●) CNOs(1750)-AIR in 0.1 mol L^{-1} NaCl; at $E = 400$ mV (vs. Ag/AgCl).

The values of C_s, calculated using Equation (2), are collected in Table 6. The specific capacitance can also be calculated using Equation (3):

$$i_c = C_s v m \quad (3)$$

The values of the specific capacitances, calculated from the dependence of the current on the sweep rates for the different samples using Equation (3), are also collected in Table 7. Clearly, the values of the specific capacitances obtained by the integration of *I–E* curves and those calculated from the linear relationship of *I–v* plots are in a good agreement.

Table 7. Specific capacitances of CNOs annealed in different environments.

Sample	C_S [F g^{-1}][a] From the integration of i_c–E voltammograms[b]	From the slope of the i_c–V relation
CNOs(1650)-N_2	35.5	36.2
CNOs(1750)-N_2	32.1	33.9
CNOs(1650)-AIR	42.6	41.9
CNOs(1750)-AIR	37.5	38.1
CNOs(1750)-CO_2	35.6	37.4

[a] Supporting electrolyte: 0.1 M NaCl; [b] Integration: ΔE between 100 and 400 mV (vs. Ag/AgCl) at a sweep rate of 20 mV s^{-1}.

Analysis of the specific capacitances shows that the second annealing modification did not significantly change the electrochemical properties of the carbon nanoparticle films. On the other hand, additional annealing leads to structural changes. Annealing under air improves wetting by creating oxygen-terminated CNO surfaces and affects the electrochemical properties. These structural and textural changes slightly affected the electrochemical properties of CNOs(1650)-AIR or CNOs(1750)-AIR and improved the penetration of the supporting electrolyte into the films.

3. Conclusion

The key factors that dictate the selection of carbon materials for supercapacitors are: structure, surface area, wettability and the presence of electroactive species. Combined thermal, spectroscopic and electrochemical analyses provide deep insights into the annealing-induced structural modifications of CNOs. The research presented here can be summarized as follows:

a) The structure and shape of the CNOs were changed as a consequence of additional annealing. This process changes the carbon structures into predominantly higher ordered graphitic layers and also causes damage and structural changes on the carbon surfaces by disrupting the graphene sheet structures, mainly after annealing under a CO_2 atmosphere.
b) An increase in line width of the *D* band suggests a higher disorder for the samples obtained at 1750 °C.
c) For the materials prepared at 1650 °C under a He atmosphere, the *G* band is closer to the theoretical position for graphite, compared with compounds obtained at 1750 °C.
d) The CNOs(1650)-N_2 and CNOs(1650)-AIR samples are more graphitic and have more ordered shells compared to CNOs(1750)-N_2 and CNOs(1750)-AIR.
e) Two prominent bands at 1430 and 1182 cm^{-1} were identified as belonging to the innermost shell of C_{60}.
f) A comparison of the specific capacitance values shows that the second modification slightly changes the electrochemical properties of the carbon nanoparticle films.
g) Taking into consideration the spectroscopic, textural, and electrochemical properties, the best characteristics for supercapacitor electrodes are exhibited by the CNOs(1650)-AIR and CNOs(1750)-AIR samples.

Experimental Section

Materials

All chemicals and solvents were commercially available and were used without further purification. Aqueous solutions were prepared with deionized water having a resistivity of 18.2 MΩ from Millipore. "*Small*" CNOs were obtained by annealing a nanodiamond powder (Molto, 5 nm average particle size) under a positive pressure of helium. A commercially available nanodiamond powder (Carbodeon μDiamond®Molto) with a crystal size of 4–6 nm and a nanodiamond content ≥97 wt.% was used as received. Annealing of ultradispersed nanodiamonds was performed at 1650 or 1750 °C under a He atmosphere with a heating ramp of 20 °C min^{-1}. The final temperature was maintained for one hour, then the material was slowly cooled to room temperature over a period of one hour. The furnace was opened and the trans-

formed CNOs were annealed in N_2, air or CO_2 at 450 (for CNOs obtained in N_2 or air) or 750 °C (for CNOs obtained in CO_2).

Methods

The films were imaged by secondary electron SEM using an S-3000N scanning electron microscope from FEI Tecnai G2 20 X-TWIN (Tokyo, Japan). The accelerating voltage of the electron beam was either 15 or 20 keV; the TEM point resolution was 0.25 nm, the TEM line resolution was 0.144 nm, the maximum diffraction angle was $\pm 12^{\circ}$, and the working distance was 10 mm. TEM images were recorded using the FEI Tecnai™ instrument. The accelerating voltage of the electron beam was 200 keV. Thermogravimetric experiments were performed using an SDT 2960 for simultaneous TGA-DTG-DTA (TA Instruments company). The spectra were collected at 10 °C min^{-1} in an air atmosphere (100 mL min^{-1}).

Diffuse reflectance infrared Fourier transform (DRIFTS)–FTIR Measurements: FTIR spectra were recorded between 550 and 4000 cm^{-1} using a Thermo Scientific Nicolet™ 6700 spectrometer at room temperature under N_2 atmosphere. The spectra were collected at a resolution of 4 cm^{-1}, apodized with a triangular function, and a zero-filling factor of one was applied. All the spectra were corrected with conventional software to cancel the variation of the analyzed thickness with the wavelength. DRIFTS spectra were recorded using a Spectra-Tech diffuse reflectance accessory equipped with the Si-Carb Sampling Kit (Spectra-Tech Inc., USA). The sample was analyzed directly on the sample cup after roughing it with abrasive paper. A small disc of silicon carbide paper was used to roughen the sample to be analyzed. Pieces of clean silicon carbide paper were used as the background. Sample spectra were referenced against a background spectrum. The spectra were transformed into reflectance units which are generally equivalent to an absorbance scale.

Room-temperature Raman spectra in the range between 100 and 3500 cm^{-1} were taken using a Jobin Yvon HORIBA LabRAM HR 800 confocal spectrometer containing a liquid-N_2-cooled charge coupled device (CCD) and two lasers: a Stabilite 2017 (Ar+ ion laser) and a He–Ne laser. To avoid sample overheating, the laser power at 633, 514, and 488 nm wavelength was less than 2 mW. The positions of the Raman peaks were calibrated using a Si thin film as an external standard. The spectral resolution of the Raman spectra was 2 cm^{-1}. The position and integral intensity of the Raman lines were obtained after computer deconvolution of the spectra using the commercial program PeakFit.

Prior to gas adsorption analysis, all samples were degassed at 350 °C at low vacuum (10 μm Hg) for 20 h to remove any adsorbed species. N_2 gas adsorption measurements were performed using a Micromeritics apparatus (ASAP2020 - automatic sorption analyzer, Micromeritics Corp., USA) at −196 °C.

Voltammetric experiments were performed using a potentiostat/galvanostat model AUTOLAB (Utrecht, The Netherlands) with a three-electrode cell. The AUTOLAB system was controlled with the GPES 4.9 software of the same manufacturer. A glassy carbon disk (GCE) with a diameter of 1.6 mm (Bioanalytical Systems Inc.) was used as the working electrode. The surface of the electrode was polished using extra fine carborundum paper (Buehler) followed by 0.3 μm alumina and 0.25 μm diamond polishing compound (Metadi II, Buehler). The electrode was then sonicated in water to remove traces of alumina from the metal surface, washed with water, and dried. The counter electrode was made from platinum mesh (0.25 mm) and was cleaned by heating in a flame for approximately 30 seconds. A silver wire with deposited AgCl, separated from the working solution by a ceramic tip (Bioanalytical Systems Inc.), served as the reference electrode.

Acknowledgements

We gratefully acknowledge financial support from the National Science Centre, Poland, grants: #2011/01/B/ST5/06051 and #2012/05/E/ST5/03800 to M.E.P.B. L.E. thanks the Robert A. Welch Foundation for an endowed chair, grant #AH-0033 and the US NSF, grants: CHE-1205302 and CHE-1408865. SEM, TEM, TGA and AUTOLAB were funded by European Funds for Regional Development, as part of the Operational Programme Development of Eastern Poland 2007–2013, project: POPW.01.03.00–20–034/09.

Keywords: capacitance · carbon nano-onions · electrochemistry · spectroscopy · structure

[1] a) J. K. McDonough, A. I. Frolov, V. Presser, J. Niu, Ch. H. Miller, T. Ubieto, M. V. Federov, Y. Gogotsi, *Carbon* **2012**, *50*, 3298; b) L. Eliad, G. Salitra, A. Soffer, D. Aurbach, *Langmuir* **2005**, *21*, 3198; c) R. Lin, P. Huang, J. Segalini, C. Largeot, P. L. Taberna, J. Chmiola, Y. Gogotsi, P. Simon, *Electrochim. Acta* **2009**, *54*, 7025; d) E. Raymundo-Pinero, K. Kierczek, J. Machnikowski, F. Beguin, *Carbon* **2006**, *44*, 2498; e) J. Chmiola, C. Largeot, P.-L. Taberna, P. Simon, Y. Gogotsi, *Angew. Chem. Int. Ed.* **2008**, *47*, 3392; *Angew. Chem.* **2008**, *120*, 3440.

[2] a) M. Kaempgen, C. K. Chan, J. Ma, Y. Cui, G. Gruner, *Nano Lett.* **2009**, *9*, 1872; b) C. M. Aguirre, C. Ternon, M. Paillet, P. Desjardins, R. Martel, *Nano Lett.* **2009**, *9*, 1457; c) S. N. Barman, M. C. LeMieux, J. Baek, R. Rivera, Z. Bao, *ACS Appl. Mater. Interfaces* **2010**, *2*, 2672.

[3] a) S. Vaziri, G. Lupina, C. Henkel, A. D. Smith, M. Östling, J. Dabrowski, G. Lippert, W. Mehr, M. C. Lemme, *Nano Lett.* **2013**, *13*, 1435; b) C. Zeng, E. B. Song, M. Wang, S. Lee, C. M. Torres, Jr., J. Tang, B. H. Weiller, K. L. Wang, *Nano Lett.* **2013**, *13*, 2370; c) J. Qin, C. He, N. Zhao, Z. Wang, C. Shi, E.- Z. Liu, J. Li, *ACS Nano* **2014**, *8*, 1728; d) K. H. Park, D. Lee, J. Kim, J. Song, Y. M. Lee, H.-T. Kim, J.-K. Park, *Nano Lett.* **2014**, *14*, 4306.

[4] a) B. B. Owens, T. Osaka, *J. Power Sources* **1997**, *68*, 173; b) E. Frackowiak, F. Beguin, *Carbon* **2001**, *39*, 937; c) E. Frackowiak, *Phys. Chem. Chem. Phys.* **2007**, *9*, 1774.

[5] R. Al-Jishi, G. Dresselhaus, *Phys. Rev. B* **1982**, *26*, 4514.

[6] a) D. M. Ugarte, *Nature* **1992**, *359*, 707; b) S. Iijima, *J. Cryst. Growth* **1980**, *50*, 675; c) V. V.; Roddatis, V. L. Kuznetsov, Y. V. Butenko, D. S. Su, R. Schlögl, *Phys. Chem. Chem. Phys.* **2002**, *4*, 1964; Roddatis, V. L. Kuznetsov, Y. V. Butenko, D. S. Su, R. Schlögl, *Phys. Chem. Chem. Phys.* **2002**, *4*, 1964; d) Ch. Jin, K. Suenaga, S. Iijima, *J. Phys. Chem. A J. Phys. Chem. B J. Phys. Chem. C Lett.* **2009**, *113*, 5043; e) N. Sano, H. Wang, I. Alexandrou, M. Chhowalla, K. B. K. Teo, G. A. J. Amaratunga, K. Limura, *J. Appl. Phys.* **2002**, *92*, 2783; f) Ch. Zhang, J. Li, E. Liu, C. He, C. Shi, X. Du, R. H. Hauge, N. Zhao, *Carbon* **2012**, *50*, 3513; g) C. N. He, C. S. Shi, X. W. Du, J. J. Li, N. Q. Zhao, *J. Alloys Compd.* **2008**, *452*, 258.

[7] a) V. L. Kuznetsov, A. L. Chuvilin, Y. V. Butenko, I. Y. Malkov, V. M. Titov, *Chem. Phys. Lett.* **1994**, *222*, 343; b) J. Qian, C. Pantea, J. Huang, T. W. Zerda, Y. Zhao, *Carbon* **2004**, *42*, 2691; c) S. Tomita, M. Fujii, S. Hayashi, K. Yamamoto, *Diamond Relat. Mater.* **2000**, *9*, 856; d) Q. Zou, Y. G. Li, B. Lv, M. Z. Wang, L. H. Zou, Y. C. Zhao, *Inorg. Chem.* **2010**, *46*, 127.

[8] a) N. Sano, H. Wang, M. Chhowalla, I. Alexandrou, G. A. J. Armatunga, *Nature* **2001**, *414*, 506; b) N. Sano, H. Wang, I. Alexandrou, M. Chhowalla, K. B. K. Teo, G. A. J. Armatunga, *J. App. Phys.* **2002**, *92*, 2783; c) I. Alexandrou, H. Wang, N. Sano, G. A. J. Armatunga, *J. Chem. Phys.* **2004**, *120*, 1055.

[9] M. Choucair, J. A. Stride, *Carbon* **2012**, *50*, 1109.

[10] T. Cabioc'h, M. Jaouen, E. Thune, P. Guerin, C. Fayoux, M. F. Denanot, *Surf. Coat. Technol.* **2000**, *128*, 43.

[11] a) X. H. Chen, F. M. Deng, J. X. Wang, H. S. Yang, G. T. Wu, X. B. Zhang, J. C. Peng, W. Z. Li, *Chem. Phys. Lett.* **2001**, *336*, 201; b) A. G. Nasibulin, A. Moisala, D. P. Brown, E. I. Kauppinen, *Carbon* **2003**, *41*, 2711; c) Y. Z.

Yang, X. G. Liu, B. S. Xu, *J. Mater. Res.* **2008**, *23*, 1393; d) C. G. Zhang, J. J. Li, C. S. Shi, E. Z. Liu, X. W. Du, N. Q. Zhao, *Carbon* **2011**, *49*, 1151.
[12] a) M. Choi, I. S. Altman, Y-J. Kim, P. V. Pikhitsa, S. Lee, G.-S. Park, T. Jeong, J.-B. Yoo, *Adv. Mater.* **2004**, *16*, 1721; b) T. Gorelik, S. Urban, F. Falk, U. Kaiser, U. Glatzel, *Chem. Phys. Lett.* **2003**, *373*, 642; c) L. Hu, S. Wang, B. Zhang, Y. Zeng, *Carbon* **2006**, *44*, 1725; d) Y. Gao, Y. S. Zhou, J. B. Park, H. Wang, X. N. He, H. F. Luo, *Nanotechnology* **2011**, *22*, 165604.
[13] J. Suehiro, K. Imasaka, Y. Ohshiro, G. Zhu, M. Hara, N. Sano, *Jpn J. Appl. Phys.* **2003**, *42*, L1483.
[14] T. Gangadhar, V. I. Bhoi, S. Kumar, C. N. Murthy, *J. Inclusion Phenom. Macrocyclic Chem.* **2014**, *79*, 215.
[15] T. Pichler, M. Knupfer, M. S. Golden, J. Fink, T. Cabioc'h, *Phys. Rev. B* **2001**, *63*, 155415.
[16] a) C. Portret, G. Yushin, Y. Gogotsi, *Carbon* **2007**, *45*, 2511; Y. Liu, Y. Kim, *Electrochim. Acta* **2014**, *139*, 82.
[17] D. Pech, M. Burnett, H. Durou, P. Huang, V. Mochalin, Y. Gogotsi, P.-L. Taberna, P. Simon, *Nat Nanotechnol* **2010**, *5*, 651.
[18] C. Portret, J. Chmiola, Y. Gogotsi, S. Park, K. Lian, *Electrochim. Acta* **2008**, *53*, 7675.
[19] S. Sek, J. Breczko, M. E. Plonska-Brzezinska, A. Z. Wilczewska, L. Echegoyen, *ChemPhysChem* **2013**, *14*, 96.
[20] M.-S. Wang, D. Goldberg, Y. Bando, *ACS Nano* **2010**, *4*, 4396.
[21] Y. Gao, Y. S. Zhou, M. Qian, X. N. He, J. Redepenning, P. Goodman, H. M. Li, Y. F. Lu, *Carbon* **2013**, *51*, 52.
[22] V. L. Kuznetsov, Y. V. Butenko, *Synthesis properties and applications of ultrananocrystalline diamond, Volume 192* (Eds.: D. M. Gruen, O. A. Shenderova, A. Y. Vul'), Springer **2005**, p. 199.
[23] E. G. Bushueva, P. S. Galkin, A. V. Okotrub, L. G. Bulusheva, N. N. Gavrilov, V. L. Kuznetsov, S. I. Moiseekov, *Phys. Status Solidi B* **2008**, *245*, 2296.
[24] M. E. Plonska-Brzezinska, A. Lapinski, A. Z. Wilczewska, A. T. Dubis, A. Villalta-Cerdas, Winkler, K. L. Echegoyen, *Carbon* **2011**, *49*, 5079.
[25] a) M. E. Plonska-Brzezinska, M. Lewandowski, M. Błaszyk, A. Molina-Ontoria, T. Luciński, L. Echegoyen, *ChemPhysChem* **2012**, *13*, 4134; b) M. E. Plonska-Brzezinska, L. Echegoyen, *J. Mater. Chem. A* **2013**, *1*, 13703.
[26] S. Tomita, A. Burian, J. C. Dore, D. Lebolloch, M. Fujii, S. Hayashi, *Carbon* **2002**, *40*, 1469.
[27] A. V. Okotrub, L. G. Bulusheva, V. L. Kuznetsov, Y. V. Butenko, A. L. Chuvilin, M. I. Heggie, *J. Phys. Chem. A* **2001**, *105*, 9781.
[28] V. Y. Osipov, A. V. Baranov, V. A. Ermakov, T. L. Makarova, L. F. Chungong, A. I. Shames, *Diamond Relat. Mater.* **2011**, *20*, 205.
[29] K. Bogdanov, A. Fedorov, V. Osipov, T. Enoki, K. Takai, T. Hayashi, V. Ermakov, S. Moshkalev, A. Baranov, *Carbon* **2014**, *73*, 78.
[30] M. Kosaka, T. W. Ebbesen, H. Hiura, K. Tanigaki, *Chem. Phys. Lett.* **1995**, *233*, 47.
[31] Y. A. Kim, T. Hayashi, K. Osawa, M. S. Dresselhaus, M. Endo, *Chem. Phys. Lett.* **2003**, *380*, 319.
[32] S. Osswald, E. Flahaut, E. H. Ye, Y. Gogotsi, *Chem. Phys. Lett.* **2005**, *402*, 422.
[33] J. G. Wiltshire, A. N. Khlobystov, L. J. Li, S. G. Lyapin, G. A. D. Briggs, R. J. Nicholas, *Chem. Phys. Lett.* **2004**, *386*, 239.
[34] J. Kastner, T. Pichler, H. Kuzmany, S. Curran, W. Blau, D. N. Weldon, M. Delamesiere, S. Draper, H. Zandbergen, *Chem. Phys. Lett.* **1994**, *221*, 53.
[35] a) Y. G. Wang, S. P. Lau, B. K. Tay, X. H. Zhang, *J. App. Phys.* **2002**, *92*, 7253; b) P. H. Tan, L. An, L. Q. Liu, Z. X. Guo, R. Czerw, D. L. Carroll, P. M. Ajayan, N. Zhang, H. L. Guo, *Phys. Rev. B* **2002**, *66*, 245410.
[36] M. Hulman, R. Pfeiffer, H. Kuzmany, *New J. Phys.* **2004**, *6*, 1.
[37] C. Thomsen, S. Reich, *Phys. Rev. Lett.* **2000**, *85*, 5214.
[38] R. Saito, A. Jorio, A. G. Souza Filho, G. Dresselhaus, M. S. Dresselhaus, M. A. Pimenta, *Phys. Rev. Lett.* **2002**, *88*, 027401.
[39] J. Maultzsch, S. Reich, C. Thomsen, *Phys. Rev. B* **2004**, *70*, 155403.
[40] M. M. Lucchese, F. Stavale, E. H. Martins Ferreira, C. Vilani, M. V. O. Moutinho, R. B. Capaz, C. A. Achete, A. Jorio, *Carbon* **2010**, *48*, 1592.
[41] F. Tuinstra, J. L. Koenig, *J. Chem. Phys.* **1970**, *53*, 1126.
[42] R. J. Nemanich, G. Lucovsky, S. A. Solin, *Mater. Sci. Eng.* **1977**, *31*, 157.
[43] R. Tsu, J. H. Gonzalez, I. G. Hernandez, *Solid State Commun.* **1978**, *27*, 507.
[44] S. A. Solin, A. K. Ramdas, *Phys. Rev. B* **1970**, *1*, 1687.
[45] a) E. D. Obraztsova, M. Fujii, S. Hayashi, V. L. Kuznetsov, Y. V. Butenko, A. L. Chuvilin, *Carbon* **1998**, *36*, 821; b) W. S. Bacsa, W. A. De Heer, D. Ugarte, A. Châtelain, *Chem. Phys. Lett.* **1993**, *211*, 346.
[46] L. G. Cançado, K. Takai, T. Enoki, M. Endo, Y. A. Kim, H. Mizusaki, *Appl. Phys. Lett.* **2006**, *88*, 163106.
[47] a) M. Yoshikawa, G. Katagiri, H. Ishida, A. Ishitani, T. Akamatsu, *Appl. Phys. Lett.* **1988**, *52*, 1639; b) M. Yoshikawa, G. Katagiri, H. Ishida, A. Ishitani, T. Akamatsu, *J. Appl. Phys.* **1988**, *64*, 6464; c) M. A. Tamor, J. A. Haire, C. H. Wu, K. C. Hass, *Appl. Phys. Lett.* **1989**, *54*, 123; d) M. Yoshikawa, N. Nagai, M. Matsuki, H. Fukuda, G. Katagiri, H. Ishida, A. Ishitani, I. Nagai, *Phys. Rev. B* **1992**, *46*, 7169.
[48] O. O. Mykhaylyk, Y. M. Solonin, D. N. Batchelder, R. Brydson, *J. Appl. Phys.* **2005**, *97*, 074302.
[49] H. Richter, Z. P. Wang, L. Ley, *Solid State Commun.* **1981**, *39*, 625.
[50] A. E. Aleksenskii, M. V. Baidakova, A. Y. Vul, V. Y. Davydov, Y. A. Pevtsova, *Phys. Solid State* **1997**, *39*, 1007.
[51] D. Baowan, N. Thamwattan, J. M. Hill, *Eur. Phys. J. D* **2007**, *44*, 117.
[52] I. V. Ponomareva, L. A. Chernozatonskii, *Microelectron. Eng.* **2003**, *69*, 625.
[53] a) G. Wang, L. Zhang, J. Zhang, *Chem. Soc. Rev.* **2012**, *41*, 797; b) V. Presser, M. Heon, Y. Gogotsi, *Adv. Funct. Mater.* **2011**, *21*, 810; c) P. Simon, Y. Gogotsi, *Philos. Trans. R. Soc. London Ser. A* **2010**, *368*, 3457.
[54] J. S. Huang, B. G. Sumpter, V. Meunier, G. Yushin, C. Portret, Y. Gogotsi, *J. Mater. Res.* **2010**, *25*, 1525.
[55] R. Lin, P.-L. Taberna, S. Fantini, V. Presser, C. R. Perez, F. Malbosc, N. L. Rupeinghe, K. B. K. Teo, Y. Gogotsi, P. Simon, *J. Phys. Chem. Lett.* **2011**, *2*, 2396.
[56] S. Brunauer, P. H. Emmett, E. Teller, *J. Am. Chem. Soc.* **1938**, *60*, 309.
[57] E. P. Barrett, L. G. Joyner, P. P. Halenda, *J. Am. Chem. Soc.* **1951**, *73*, 373.
[58] a) Y. Oren, A. Soffer, *J. Electroanal. Chem.* **1985**, *186*, 63; b) Y. Oren, H. Tobias, A. Soffer, *J. Electroanal. Chem.* **1984**, *162*, 87; c) M. Yaniv, A. Soffer, *J. Electrochem. Soc.* **1976**, *123*, 506; d) J. Koresh, A. Soffer, *J. Electrochem. Soc.* **1974**, *124*, 1379; e) J. S. Newman, C. W. Tobias, *J. Electrochem. Soc.* **1962**, *109*, 1183; f) R. DeLevie, *Electrochim. Acta* **1964**, *9*, 1231.

Received: January 22, 2015
Published online on May 28, 2015